Impact of Variable Channel Conditions on Multi-Hop DTN-Based Lunar Communications with Traffic Prioritization

Klara Schaper, Teresa Algarra Ulierte, Andreas Timm-Giel
Institute of Communication Networks, Hamburg University of Technology, Hamburg (Germany)
e-mail: research@klaraschaper.de, {teresa.algarra.ulierte | timm-giel}@tuhh.de

Felix Flentge
Directorate of Operations, European Space Agency, Darmstadt (Germany)
e-mail: felix.flentge@esa.int

***Abstract*—The Moon is the closest object in space to Earth, and therefore of high value for space research. This can be seen in the numerous planned missions involving the Moon, which will require a stable and robust infrastructure for Earth-to-Moon communication. The existing architectures and protocols — Delay- and Disruption-Tolerant Network (DTN) and Bundle Protocol (BP) — were designed for the challenges of space communication. Nevertheless, they currently lack Quality of Service (QoS) assessments to provide a stable link under high transmission rates and limited bandwidth. One promising solution is the use of traffic prioritization, which has been shown in previous work to improve the performance for a limited amount of critical information bundles at the expense of bulk bundles. This research builds on the aforementioned previous work to model a multi-hop Earth-to-Moon communication path, accounting for differences in space and atmospheric link characteristics and error sources, and extends the work previously published [1]. Through a set of simulations, traffic prioritization was evaluated for one-hop, two-hop and three-hop paths together with optimal, average and worst conditions of the link. An impactful performance improvement was found for high priority bundles throughout all the experiments. In addition, it was found that the efficiency of the high priority packets decreased as the number of hops increased, while the exact opposite was observed for the low priority packets. The study recommends traffic prioritization for time-sensitive data and highlights the need to incorporate priority in routing decisions to enhance QoS.**

Keywords-Solar System Internet (SSI); Space Communications; Delay- and Disruption Tolerant Network (DTN); Bundle Protocol (BP); Quality of Service (QoS); Traffic Prioritization

I. Introduction

The Moon, being the nearest celestial body to Earth, plays a vital role in the future of space exploration [2]. This is particularly evident through the growing number of planned missions and satellite deployments by European Space Agency (ESA), National Aeronautics and Space Administration (NASA), Japan Aerospace Exploration Agency (JAXA) and Indian Space Research Organisation (ISRO) among others. The presence of a reliable communication network is essential for the success of these missions. This is an especially challenging task in the context of space communication, since the characteristics of the communication link in space are marked by intermittent connectivity, long or variable delays, asymmetric data rates and high error rates.

To overcome these obstacles, the concepts of Delay- and Disruption-Tolerant Network (DTN) and Bundle Protocol (BP) were created. Their main feature is their packet-switching approach, this solving the problems of no end-to-end paths, intermittent connectivity and the long delays [3]. However, certain challenges remain unresolved, particularly the bandwidth limitations caused by the high demand from the numerous aforementioned missions. A prominent example of this challenge is the Lunar Gateway — the first space station to orbit beyond Earth — which is intended to function as a communication relay between Earth and the Moon. The European System Providing Refueling, Infrastructure and Telecommunications (ESPRIT) module of the Lunar Gateway is expected to provide a maximum bandwidth of $25\,\mathrm{Mbit\,s^{-1}}$ [4], yet an average scientific mission will presumably consume up to $20\,\mathrm{Mbit\,s^{-1}}$ [5]. When combined with telemetry, tracking and command (TT&C), essential communications, and multiple science missions, this demand is likely to exceed the available bandwidth, resulting in significant queuing delays and potential data loss.

To maximize the utilization of such limited bandwidth, traffic prioritization, a Quality of Service (QoS) mechanism, can be used as a mitigation strategy by prioritizing urgent data. Such a system is however not included in the BP specification, but a theoretical approach exists to include this and several other QoS parameters into an extension block, researched by Algarra et al. [6]. Especially with traffic prioritization they showed a significant enhancement in the delay of high priority bundles [7]. The issue with this research is that a direct Earth-to-Moon transmission path is assumed. Many of the missions will not be equipped with a Direct-to-Earth communication link [8], but will depend on relay satellites to increase the frequency of communication windows, or to have it at all in the case of missions targeting the far side of the Moon. For such missions, deploying and utilizing relay satellites is essential to establish connectivity. As a result, a more realistic analysis that incorporates

multi-hop communication paths is necessary.

The purpose of the original paper [1] was to analyze the effect of traffic prioritization on multi-hop Moon-to-Earth communication links. To achieve that the model of Algarra et al. [6] was adapted to allow flexible numbers of hops, enabling representation of diverse multi-hop paths and future use cases. These modifications necessitated re-evaluating traffic prioritization in DTN using the BP. The adapted model was then used in simulations to compare bundle transmission delays across three priority classes with a non-prioritized scenario. Since this work extends the original all these propositions remain accurate with an additional focus on the link through various conditions. This not only enables a deeper evaluation of traffic prioritization but also allows for additional insights into traffic routing and the overall link performance, building on observations from the original work.

The structure of this paper is as follows: Section II provides the necessary background information, covering topics such as DTN, BP, QoS, and Markov chains. Subsequently, the work of Algarra et al. [6] is discussed in Section III, along with other relevant studies. The adapted model and its key components are detailed in Section IV. Section V presents the analysis and evaluation of the experiments conducted using the implemented model. Finally, Section VI summarizes the findings and outlines directions for future research.

II. Background

Space communication networks face unique challenges that distinguish them from terrestrial systems. To address these challenges, specialized protocols and architectures have been developed, forming the foundation for reliable Earth-to-space communication links.

A. DTN

The characteristics of communication links in space are marked by several challenges which are not present in terrestrial communications: lack of end-to-end path, intermittent connectivity, long or variable delays, asymmetric data rates and high error rates. Traditional internet protocols, designed for terrestrial networks with stable end-to-end connectivity, fail to operate effectively under these conditions. The DTN was created to provide a reliable communication link in environments where these challenging conditions occur. Its key innovation is the store-and-forward message switching mechanism, which replaces the end-to-end path assumption of terrestrial internet protocols. With this approach, the entire message or parts of it are moved from one persistent storage node to the next, enabling a more suitable hop-by-hop communication method as illustrated in Figure 1 [3].

Since end-to-end paths are not guaranteed in space environments, messages can be stored at intermediate nodes until a communication link becomes available. This approach ensures that packet delivery is always faster

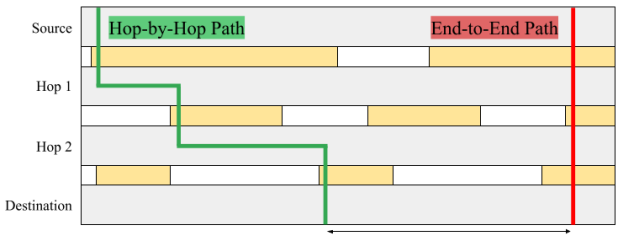

Figure 1. Hop-By-Hop vs End-To-End

than traditional methods or, in the worst case, equally fast, making it particularly valuable for cases in which connectivity windows are limited and unpredictable [3].

B. BP

The store-and-forward message switching capability of DTN is implemented through BP. It operates as an overlay layer positioned below the application layer and above the transport layer, as shown in Figure 2. This architecture allows for terrestrial protocols to still be used even under the circumstances present in space environments. Additionally, this approach preserves compatibility with existing network infrastructures, making BP conveniently interoperable [3].

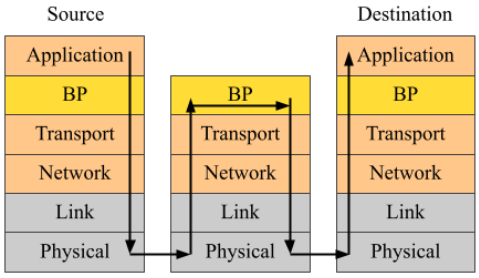

Figure 2. Bundle Protocol (BP)

In BP, messages to be transmitted are encapsulated into a bundle, which contain both the payload data and the metadata required for successful transmission across the network and proper decoding at the destination. Each bundle consists of three types of blocks:

- Primary Bundle Block: contains essential information such as the source node ID, destination node ID, and the bundle's creation time. This block is protected against modification using the Block Integrity Block (BIB) [9].
- Extension Blocks: optional blocks that provide supplementary information, such as the bundle's age or hop count. Since these are not mandatory, some intermediate nodes may be unable to interpret or process specific extension blocks.
- Payload Block: holds the actual data being transmitted. To ensure its integrity, this block is also protected by the BIB.

This bundle structure, combined with the store-and-forward mechanism, enables reliable data transmission across the challenging space communication environment

while maintaining compatibility with existing network protocols and infrastructure.

III. Related work

This section reviews existing approaches to QoS in space communications, their modelling and characterization, and establishes the foundation for our multi-hop analysis.

A. QoS and Channel Modelling for DTN

Space channels are highly stressed communication environments, with periods of extremely low Frame Error Rate (FER) that can abruptly transition into outages lasting from minutes to hours [10]. This high variability and prolonged downtime render conventional terrestrial QoS approaches unsuitable for space communications. Just as DTNs developed to address the unique challenges of space links, tailored QoS mechanisms are required to ensure reliable performance under these extreme conditions.

One of the approaches that been demonstrated as an effective mechanism to mitigate the impacts of space channel volatility is traffic prioritization. It was first implemented in BP with the Class of Service block for DTNs defined in RFC 5050 [11], which includes "expedited", "bulk" and "normal" classes. However, this classification proved to be inadequate, resulting in the formulation of the Extended Class of Service (ECOS) block with which the classes "critical", "streaming", "ordinal", and "reliable" were added. While defined in the Consultative Committee for Space Data Systems (CCSDS) BP Specification [12], ECOS still had significant limitations, mainly the inflexibility caused by the predefined usage of each class, as well as the lack of adaptability due to the inclusion of retransmission schemes within traffic prioritization [12]. Though ECOS did not get standardized, it was implemented in the Interplanetary Overlay Network (ION) [13].

Building on this foundation, Apollonio et al. [14] investigated the integration of ECOS with Contact Graph Routing (CGR), the routing algorithm used in DTN with BP. They tested flags such as "streaming", "bulk", "expedited", and "critical" for a communication path from Earth to the far side of the Moon. Each flag was handled optimally by CGR algorithm: "streaming" bundles followed the best routes, "bulk" bundles made the most of limited bandwidth, and "critical" bundles were sent earlier, postponing lower-priority traffic. This work demonstrates the potential benefits of traffic prioritization in space environments. However, it assumed uniform loss rates, whereas real-world conditions exhibit both uncorrelated (e.g., thermal loss) and correlated losses (e.g., atmospheric or solar effects). This work addresses this limitation by using a multi-hop model with more accurate loss characteristics to validate results under more realistic conditions.

Additional research has explored channel modeling for space communications. Various Markov modeling approaches have been used [15], with the most common being the Gilbert-Elliot model (2-state Markov chain) [16], where the channel alternates between a "good" and a "bad" state, providing a binary state distribution. More complex models have been applied to non-terrestrial networks, such as land mobile satellite (LMS) communications [17][18]. In these, three-state Markov chains are used to classify losses according to their severity, such as moderate or deep attenuation. Chu et al. [19] further extended this approach with a four-state Markov chain, incorporating two error and two good states. This model focused on losses across the entire low-Earth orbit path rather than on burst error sequences.

These studies support the applicability of Markov chains to space communication channels. However, they are primarily tailored for satellites and Earth-orbit scenarios, not for lunar, Martian, or deep-space links. In that regard, Pan et al. [20] provide a broad overview of deep-space channel models, categorizing them into near-Earth, interstellar, and near-planet links. For each scenario, they describe potential losses that can occur, and provide a mathematical model for those losses. While this can serve as a basis for constructing more comprehensive models, it lacks a concrete channel model combining short- and long-term losses in a way suitable for near-Earth and deep-space scenarios, which is the focus of this work.

B. Current Approach

Previous research is based on the assumption that a robust QoS approach must be created considering the space-specific challenges and link characteristics that the transmission will face [10]. To study these challenges, a channel model approach was developed using a Markov chain [6].

While the available literature already uses Markov chains to model channel behavior, such as the Gilbert-Elliott models [16] and the multi-state LMS models [17]–[19] presented in Section III-A, the novelty in our approach lies in the use of a three-state Markov chain specifically tailored for cislunar and deep-space links. The state differentiation allows for more accurate and precise depiction of all the different error sources that can be present in the channel, and makes a separation between long-term or correlated losses, and short-term or uncorrelated losses. The three states are defined as follows:

- Success state: in this state, the transmission is successfully sent by the source and received by the end node without major losses.
- Short-term loss state: here, the transmission failed due to short-term effects such as antenna pointing errors, interference, or light atmospheric phenomena.
- Long-term loss state: lastly, if the transmission fails due to long-term phenomena, the channels will suffer from burst losses that may last from several seconds up to hours. Causes for this include solar storms or severe atmospheric events.

While the three-state Markov chain has proven to model the channel more accurately than other approaches

found in the literature, the values taken in the presented previous work lacked precision. The improved Markov model presented in Section IV takes into account a wider range of error sources and models them in a more accurate and complete manner.

This model enabled the identification of key QoS parameters relevant for space scenarios, which were implemented in an extension block for BP, named the User QoS Extension Block (UQEB) [6][21]. It includes the following QoS mechanisms:

- Traffic prioritization: in order to cope with the long delays and possible bottlenecks, traffic prioritization is critical to enable time-sensitive information to arrive at their destination within the desired latency bounds. Three main classes are described: critical, normal and bulk. Within those, there are sub-priority classes which allow for fine-tuning of the latency requirements.
- Required reliability: due to the high error rates, transmissions often fail to reach their destination. Deciding whether an Acknowledgement (ACK) upon reception is required or not depends on the data that is being transmitted, as well as on the characteristics of the specific link at hand (some links might be uni-directional). This UQEB entry allows for specification of this requirement.
- Latest-only delivery: due to the intermittent connectivity and bottlenecks, it is not uncommon for bundles to accumulate at a node. For some data types, only the latest information might be relevant, such as the case of sensor networks. Should several of these bundles meet at a node, only the latest one will be forwarded and the rest will be dropped.
- Bundle storage: given that the persistent storage in the intermediate nodes is limited, a long period of no connectivity or a surge of bundles might cause the storage to run low. In this case, bundle storage allows for the user to indicate which bundles can be dropped first and which should be kept.

The feasibility studies performed using the UQEB in conjunction with the Markov chain show that the transmissions which included their QoS needs (especially priority classes) had an improved adjustment to their respective requirements: the critical and normal bundles had a shorter delay at the expense of a longer delay for bulk bundles [7][22]. However, this prior work assumed direct Earth-to-Moon visibility in the communication link, which is unrealistic for many future missions that will rely on relay satellites and multi-hop paths.

C. Contribution

As a conclusion, existing work on space channel modelling predominantly relies on simplified or uniform loss models, which do not reflect the heterogeneous nature of the channel. Furthermore, these studies generally lack a channel model capable of representing the impact of both short-term uncorrelated losses and long-term correlated losses in transmissions. To address this gap, both prior work and the present study define a channel model based on a three-state Markov chain that incorporates distinct space and atmospheric error sources (see Section IV). This work expands the previous work by considering varying conditions (optimal, average, and worse-case), enabling evaluation of the full range of potential link performance.

The second critical research gap concerns QoS for DTN and BP. Prior work has primarily evaluated traffic prioritization under the assumption of a direct Earth-to-Moon link, without considering multi-hop communication paths. This is a significant limitation, as a growing number of missions will depend on orbiters and relay satellites to establish connectivity. To address this, the present work introduces a multi-hop Earth-to-Moon channel model that enables assessment of traffic prioritization across multiple hops. This approach provides a more realistic evaluation of priority behavior in lunar communication networks (see Section V).

IV. Model

To assess traffic prioritization under realistic conditions, a comprehensive channel model must be developed which accounts for the diverse loss characteristics encountered in the scenarios at hand. This model distinguishes between different types of losses and communication settings to accurately represent the challenges faced by the communication link.

There are two fundamental types of losses:

- Uncorrelated losses: losses that occur sporadic and shortly. These arise from causes with short duration, such as thermal loss or short interferences.
- Correlated losses: losses that occur repeatedly for extended periods of time, resulting in the loss of multiple packets in a row. Such losses can be caused by atmospheric phenomena (e.g. storms) or space weather (e.g. solar flares).

To analyze the specific losses affecting the communication link, this work models a transmission path from a lunar node (e.g., astronaut, rover, or mission equipment) to an Earth ground station via relay satellites. This path encounters two distinct environments:

- Space setting:
  - Starting at the lunar source, the transmission travels through the exosphere of the Moon. Since this is a very thin layer of gas, and the atmosphere is negligible, no weather can develop. This results in no atmospheric disturbances on the surface of the Moon [23].
  - The next stage of the transmission is the travel through outer space, exposed to the Sun without any protection. While regular solar radiations are uniform and, therefore, calculable and manageable, solar storms are unpredictable.
- Atmospheric setting:
  - As the transmission approaches its destination, it encounters Earth's atmosphere, which is significantly

denser than that of the Moon. This increased density can lead to interference from atmospheric weather phenomena.

Moreover, the communication system must be defined in order to identify the applicable error sources. This can be either Radio Frequency (RF) or Free Space Optical (FSO). Due to its rising popularity, FSO is expected to be used in ground-to-Earth orbit scenarios, and RF is taken as the standard for space communications due to the long distances to be conversed [24].

With this separation of losses and settings set, the Markov model presented in Section III-B can be extended to the following one (Figure 3):

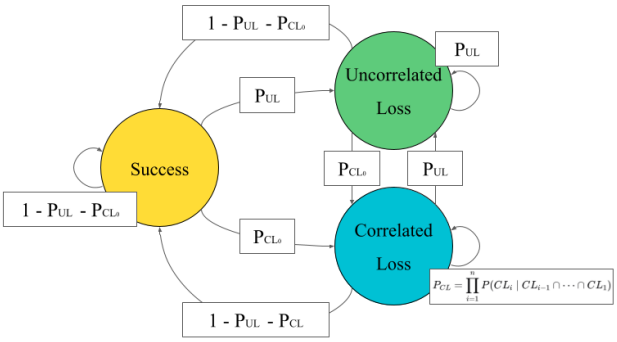

Figure 3. Complete Markov Model

The associated transition matrix to the defined Markov chain is given in Equation 2. It depends on the input parameters P_{UL}, P_{CL_0} and P_{CL}, where P_{CL} is defined in Equation 3.

$$\mathbf{P} = \begin{bmatrix} P_{S\to S} & P_{S\to UL} & P_{S\to CL} \\ P_{UL\to S} & P_{UL\to UL} & P_{UL\to CL} \\ P_{CL\to S} & P_{CL\to UL} & P_{CL\to CL} \end{bmatrix} = \tag{1}$$

$$= \begin{bmatrix} 1-P_{UL}-P_{CL_0} & P_{UL} & P_{CL_0} \\ 1-P_{UL}-P_{CL_0} & P_{UL} & P_{CL_0} \\ 1-P_{UL}-P_{CL} & P_{UL} & P_{CL} \end{bmatrix} \tag{2}$$

$$P_{CL} = \prod_{i=1}^{n} P(CL_i \mid CL_{i-1} \cap \cdots \cap CL_1) \tag{3}$$

To maintain realistic transition probabilities, the simulation employs two separate Markov chains: one representing the space setting and one representing the atmospheric setting. The boundary between these environments is taken as the International Space Station (ISS) for this work, as it is the closest fixed node to Earth, located approximately 400 km above the surface.

The losses depicted in Figure 3 are specific to each environment, and are explained in detail in Section IV-A and Section IV-B. To provide even more accuracy, the system will model three different types of conditions: optimal, average and worst. Optimal conditions feature high throughput because of low influences on the communication link. Average conditions portray more typical loss probabilities, which are higher than those presented under optimal conditions. In case of worst conditions, the probabilities for loss are as high as possible without loss of realism.

A. Space losses

To send data through RF, the digital data is encoded onto a high frequency electromagnetic wave. This output is then amplified and sent through space to the receiver, which decodes the received signal back into digital data. The frequency used depends on the needs. A higher frequency offers a higher data rate, but with the risk of higher loss, whereas with a lower frequency only lower data rates are possible, but with the advantage of a lower error rate. Since the used frequency varies significantly, no specific frequency is modeled [24].

The antenna of the sending satellite has to be aligned for any frequency band used, although the alignment precision needed depends on the frequency. The higher the frequency, the lower the tolerance for pointing errors [24]. Since pointing errors do not happen in long bursts, they can be considered as an uncorrelated loss. Satellites themselves are susceptible to small errors, especially since both solar and cosmic radiation damages the electronics by overcharging them or through high-energy particles penetrating them [25]. Such system errors are considered as uncorrelated losses, since they do not happen in bursts, but as single random losses. These two losses are simulated together in one probability with 0.0014% for optimal, 1.9% for average and 4.35% for worst case conditions. The values are taken from a study of typical satellite-to-ground systems, which models the expected erasure percentage in a transmission under several circumstances [26]. These percentages taken depict the probability of the losses being higher than 6 dB, which is the standard link budget margin used by the missions at hand.

The correlated losses considered in this work do not stem from the satellites themselves but from the environment they are in. The solar storms are caused by explosions on the Sun releasing a large amount of energy [27]. They can be categorized according to their peak brightness in X-ray wavelength and sorted by their level of impact. X-class flares have the highest impact, followed by M-class flares and then C-class flares. All three classes can have consequences on Earth, according to their level of force. The weakest flares are the B-class and A-class flares, with no influence on Earth. The effect of these solar flares on the communication is a complete blockage of the channel, since they are a burst of radiation that spreads across the electromagnetic spectrum, which includes the radio frequencies [25]. This can be depicted as a continuous transmission over all channels, blocking the medium completely for all other sending attempts.

Figure 4 illustrates this process showing how the emitted radio waves can not reach the next satellite because of the solar flares blocking the way.

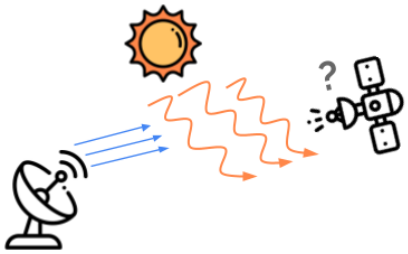

Figure 4. Influence of a Solar Storm on a RF Communication Link

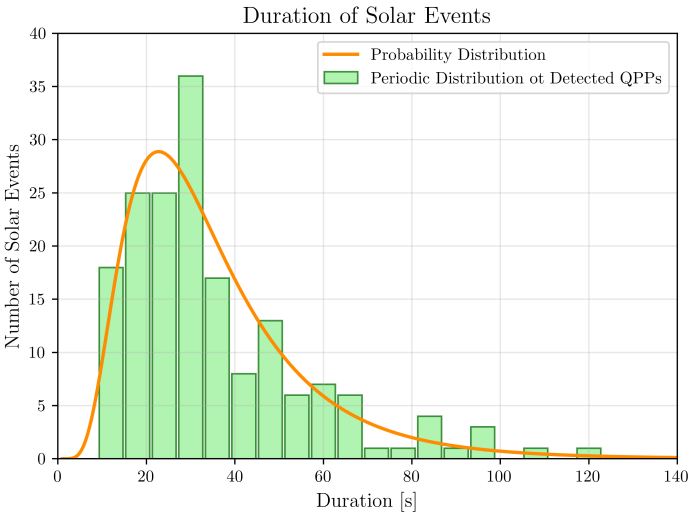

Figure 5. The Periodic Distribution of the Detected QPPs (reproduced from [29])

Solar flares can also have a direction, such that even though a solar storm is taking place, the communication might not be interrupted. Nevertheless, this research assumes solar storms to cause a general channel blockage, regardless of their direction. Regarding the level of force, only the classes X, C and M are considered to have enough impact on the communication channel. Solar storms belong to the correlated losses since they cause burst errors due to their duration being anything from seconds to minutes. Moreover, their area of impact is extensive, influencing all satellites in the path.

To determine the probability of entering a solar storm, the work of Nishizuka et al. [28] was used. They developed a forecasting model for solar storms for which they observed the occurrences of the different solar flare types in a specific time period. In the time frame of 2009 days they observed 26 X-class, 383 M-class and 4054 C-class solar flares. These numbers were used for a calculation of percentage per second. For the worst case condition all three types were included, which makes a sum of 4463 solar flares and results in an entry probability of 0.003%. The optimal case leaves out the C-class flares, since they are the weakest ones of the considered classes, and they do not necessarily block the channel, such that the sum only amounts to 818 and a probability of 0.002%. The average condition is set as a middle between those two probabilities with 0.0025%.

For the probability of staying in correlated loss in the space setting, only one curve for all three conditions is used. This curve is taken from the work of Guo et al. [29], which researched the appearances of Quasi-Periodic Pulsation (QPP) in solar flares. QPPs are a common feature of solar flares, and the graphical representation of their occurrence gives a function for the general course of a solar flare. This function can be seen in Figure 5. The x-axis gives the time in seconds, and the y-axis the number of QPPs occurring at that time.

This graph represents the length distribution of solar storms, from which we derive the probability of staying in the solar storm after a certain time. It is important to note that solar storms are always at least 6 s long, such that the probability of staying is 100% until 6 s have passed. The function follows a logarithmic normal distribution and in the simulation an approximation of the given curve is used, because the original data is not available. Since the referenced graph consists of bars, all values were normalized by multiplying them with the range of one interval, to get a continuous function from the discrete values.

B. Atmospheric Losses

As previously stated, this research has chosen to model the link as FSO, which is a technique based on optical wavelengths of electromagnetic radiation. The fundamental process is the same as in RF based communications, meaning that the data to be sent is modulated into electromagnetic waves and sent to a receiving system, but the frequency used is much higher, generally at near-infrared bands which explains the comparison to lasers. FSO offers much higher data rates than RF, even when using high-frequency bands, and it is much less likely to be jammed. However, these advantages come at the cost of some error-prone properties, from which the losses to be modeled in this link can be drawn [24].

Beginning with the uncorrelated losses, the pointing of the antenna has to be much more accurate than for RF, since the beam is narrower. Additionally, the beam does not only travel through empty space, but through the atmosphere of the Earth, with many more elements to influence a communication. The changes in the atmosphere's density and its composition of particles can scatter the beam, and thus result in loss [24]. For the pointing errors and interferences in the atmospheric setting, the probabilities from the space settings are taken again, since such losses are not dependent on the setting and should therefore be the same.

Aerosols in the atmosphere are another challenge for FSO communication. They are minute particles and can vary from liquid to gaseous. The size, concentration and origin differs and depends on the location, season, time of day, weather conditions and natural events such as volcanic eruptions or desert dust. The impact of aerosols is an attenuation of the transmission, and the amplification of

sky radiance, which is a scattering of the sunlight, such that the noise in transmissions is increased [30]. Because of its high influence, aerosols are modeled separately from atmospheric turbulence in the uncorrelated losses. Their dependence on the time of day, the weather, and the season, would also make them fitting for an inclusion into correlated losses, but the effect on the scenario at hand would be negligible in comparison to the complexity of the analysis needed, as well as the lack of available data on this topic due to said complexity. The probability for aerosols is taken from an informational report on real-time weather and atmospheric characterizations [30]. The report provided two graphs, representing the cumulative probability of loss at 1550 nm and at 1064 nm. Since the frequency was not defined for the simulation, the graph is selected based on higher probability for loss, to rather depict the worst scenario than to provide an overly optimistic view (see Figure 6). For the average case the curve for worldwide is taken at the point of 6dB loss, because it is averaging the transmission loss at 6dB over the whole world. The worst condition depicts the curve of Beijing at 6dB loss, since it is by far the curve with the slowest increase. In the optimal case there are no aerosols influencing the transmission, so the probability is taken as 0%.

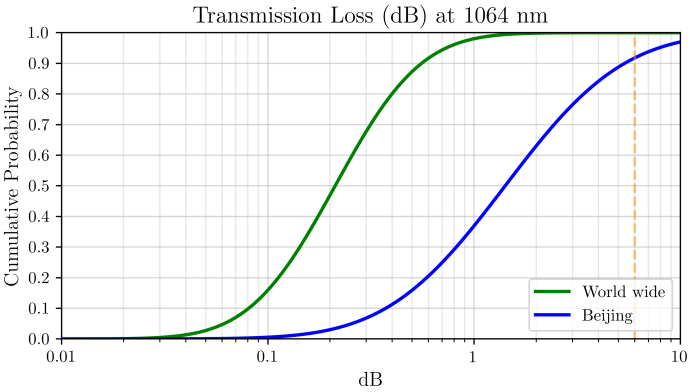

Figure 6. Transmission Loss Due to Aerosols (reproduced from [30]).

The biggest influence on FSO remains the clouds since cloud coverage has a similar effect on FSO as solar storms: Their occurrence results in a complete blockage of the channel. The moisture of the clouds causes such a large attenuation, that communication becomes impossible [24]. The water droplets and/or ice crystals that clouds consist of, scatter and absorb the optical wavelengths. The level of interruption depends on the thickness of the clouds; the thicker the cloud, the higher the disturbance. However, independent of the thickness, clouds always interfere with the communication link to some degree. Additionally, during daytime, clouds have a similar effect as aerosols in terms of scattering Sun irradiance, hence increasing the sky radiance [30]. In order to simplify the complexity that clouds present with regard to their type, size and thickness, the presence of a cloud is taken as a complete blockage of the channel. This still presents a realistic scenario since the blockage would come either from the thickness of the cloud, or from the sky radiance. Another factor to reflect in the model is the duration of clouds. Depending on the wind conditions, clouds can cover the sky from minutes to hours, resulting in a high amount of loss. Therefore, clouds are categorized as correlated loss in this model.

For the probability of entering the correlated loss state, a calculation based on the rainy days at three stations out of the ESA core network was done. Using the number of cloudy days per year as a basis would have been the optimal procedure, but unfortunately no reports on this metric were found. The optimal condition is given at Santa Maria (Portugal), with only 13 rainy days per year [31]. Converting that into a probability per second by dividing it by 365 and then by 86400, we get a probability of 0.000041% to get into the correlated loss state. For the average condition Kiruna (Sweden) was chosen with 92 days of rain per year, which results in a probability of 0.00029% per second [32]. The worst case condition is given at Kourou (French Guiana), with the number of rainy days amounting to 188, which gives a probability of 0.00043% [33].

However, the probability of staying in the correlated loss state in the atmospheric setting depends on time. The curves used can be seen in Figure 7, which depicts the probabilities of the sky staying cloudy over time. In the original work from Iver A. Lund [34] the sky cover is represented in tenths, such that 0 indicates a clear sky and 10 indicates a completely covered sky. Therefore, each curve serves as the respective tenths of the sky staying covered. The worst case would be that the sky does not clear up very much after cloud occurrence, which is characterized by the probability curve of 9 tenths of the sky staying covered. The curve of 10 tenths was intentionally excluded, because it is nearly linear and gives the clouds too high an influence in the Markov model. In the optimal case the sky clears up completely, which is the curve of 0 tenth staying covered. Lastly for the average case the curve of 5 tenth of the sky staying covered was chosen as a middle ground. The functions used in the simulation are approximations of these given curves, since the original data is not available.

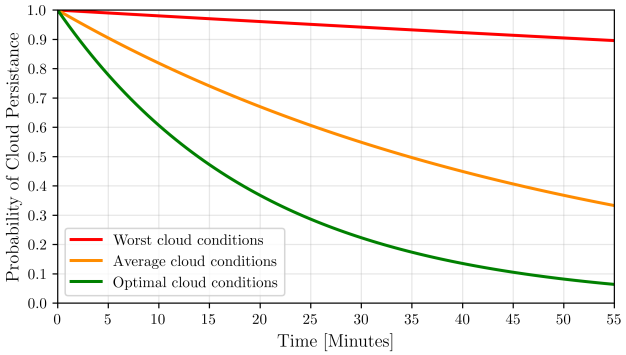

Figure 7. Cloudy Line-Of-Sight Persistence Probabilities (reproduced from [34]).

All probabilities and their affiliations are summarized in

Table I.

TABLE I. Correlated and Uncorrelated Losses for the Space and Atmospheric Settings

Setting	Loss Type		Optimal	Average	Worst
Atmospheric	Uncorrelated	Pointing errors and interferences	0.0014%	1.9%	4.35%
		Aerosols	0%	2%	5%
	Correlated	Clouds	0.000041%	0.00029%	0.00043%
Space	Uncorrelated	Pointing errors and interferences	0.0014%	1.9%	4.35%
	Correlated	Solar storms	0.002%	0.0025%	0.003%

With these values the following simulation was build and studied.

C. Simulation

The code basis of this simulation is from the work of Algarra et al. [22], which was explained in Section III-B and was kindly provided for extension to cover the adapted model.

To simulate several days within a few hours SimPy [35] is used, a process-based discrete-event simulation framework. The first two processes introduced into the SimPy environment are the Markov chains modeling the atmospheric and space conditions. Both share the same abstract structure described in Section IV, differing only in their state-transition probabilities; therefore, they are explained together.

During initialization,

- the probability of transitioning into uncorrelated loss is set based on the selected condition,
- counters for all three states (success, correlated loss, uncorrelated loss) are created, and
- the start state is set to *success*.

Each Markov-chain process then runs in a loop until the set simulation time. In each loop the probability of entering the correlated-loss state is set anew according to the condition, if the Markov-chain is currently not located in the correlated-loss state. Otherwise, this value is instead computed using the corresponding solar-storm or cloud model. The duration spent in this state needed for the computation is tracked by storing the entry time and subtracting it from the current simulation time during each update.

To get into any state, a random number in $[0, 1]$ is drawn. As seen in Figure 3, if it is below $1-P_{CL_0}-P_{UL}$ the process is in the success state; if it exceeds $1 - P_{CL_0}$ it enters the correlated loss state; otherwise, it enters uncorrelated loss. After determining the state, the process waits one second before repeating. Throughout the simulation, other processes query these Markov chains to obtain the current atmospheric or space-link state.

Once the Markov chains are running, the communication link is simulated, transmitting bundles from source to destination. Each priority class has its own traffic generator, which creates and sends bundles with IDs, priorities, and arrival timestamps. A benchmark case with no traffic prioritization (First-In-First-Out (FIFO) queuing) uses the same traffic volume for comparison. Each traffic generator begins after a random initial delay between zero and the set bundle arrival rate, preventing synchronized starts. It then runs in a loop, generating new bundles at uniform distributed intervals.

Before adding the traffic generators, the node storages are initialized to handle incoming bundles. The number of storages equals the number of hops plus one special storage called 'destination'. Initialization proceeds in reverse order so each storage knows its successor (the last one points to destination) and its predecessor (the first one receives bundles from the traffic generator). Figure 8 illustrates this setup, showing that the first node storage functions as the source, even though bundles originate from the traffic generator. Therefore, transfers from the traffic generator to the first storage do not count as hops, whereas transfers into the destination do.

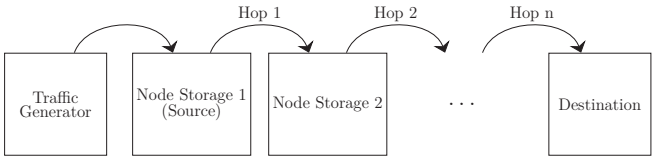

Figure 8. Structure of the Node Storages

Each storage has a 'receive' function that records bundle arrival times and adds bundles to the internal queue. The main function of each node handles forwarding: in an infinite loop, it requests the current state from the appropriate Markov chain according to the hop scenario. In case of a hop bypassing the border, both Markov chains are requested, and the state is only set to success if both chains are in the success state, otherwise resulting in a loss state. On a success, the bundle is sent to the next node after a timeout equal to the bundle service time. On a loss, the timeout is doubled, after which the bundle is resent.

The destination storage differs only in that it lacks a main forwarding function. Its 'receive' function sorts bundles by priority and records delivery statistics, while still appending the arrival time to the bundle, since the transition to the destination counts as a hop as Figure 8 demonstrated.

Throughout the whole simulation data is recorded not only for the evaluation of the results but also for the evaluation of the simulation. The number of occurrence of each state, the consecutive errors for uncorrelated and correlated loss as well as the bundle delivery rates and bundle loss ratios were recorded to check for plausibility. These verification mechanism along with the careful researched parameters ensure the authenticity of the results.

V. Results

This section presents a comprehensive evaluation of traffic prioritization performance across different multi-hop scenarios and channel conditions. Each run consists of

an experiment with critical, normal and bulk classes and an experiment with First-In-First-Out (FIFO) approach to see the impact of traffic prioritization in comparison to the benchmark. All three priority classes have the same amount of traffic and the FIFO experiment has the same amount as all priority classes together. The simulations run for 500 simulated days each to ensure enough data is collected. The parameters to configure for every experiment are the conditions and the scenario.

The condition represents the state of the communication link and changes the probabilities of the events accordingly as seen in Section IV. The modeled conditions are optimal, average and worst conditions. This range allows for a detailed analysis of the impact of traffic prioritization in different link states, and to derive where it performs best.

The experiments have the goal to reevaluate the impact of traffic prioritization on a multi-hop path. Additional focus will lie on the differences occurring between a direct path and a multi-hop path, and the conclusions that can be drawn from that for the future Moon-to-Earth communication. For that, three scenarios were chosen (see Figure 9), all depicting the expected near-future:

- Direct communication (one-hop): the distance of 405 500 km represents the Earth-Moon link at apogee. It was selected for a comparison between the work of Algarra et al. [6] and the modified model.
- Relayed communication with two hops: the distances are 70 000 km from the Moon to the Lunar Gateway, and 335 500 km from the Lunar Gateway to Earth. As highlighted in Section I, the Lunar Gateway will improve bandwidth for critical missions, making a traffic prioritization analysis on such a scenario desirable.
- Relayed communication with three hops: the distances are 70 000 km from the Moon to the Lunar Gateway, 335 100 km from the Lunar Gateway to the ISS, and 400 km from the ISS to the ground station on Earth. Since the ISS was chosen as the boundary between the atmospheric and the space setting in the modeling, this scenario strictly separates the environments, such that each link only corresponds to one setting.

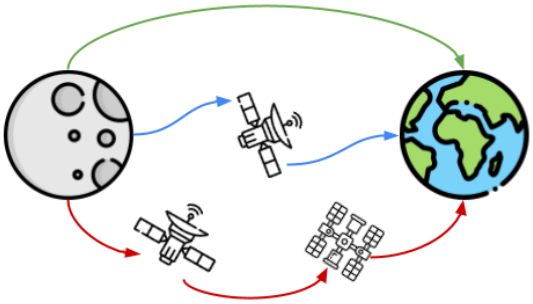

Figure 9. One-Hop Scenario (Green), Two-Hop Scenario (Blue) and Three-Hop Scenario (Red).

The results from all experiments are analyzed in detail in the following subsections, organized by scenario type with comparative analysis across different channel conditions. Focus of the analysis is the end-to-end delay of each bundle generated at a rate sufficient to prevent queuing under ideal conditions. The Cumulative Distribution Function (CDF) graphs illustrate the percentage of bundles that arrive within a given time threshold. Of particular interest are the 2.5 s and 5 s marks, representing the threshold defined by ESA for qualifying as normal communication, and twice that threshold, respectively, for reference [6].

A. One-Hop Scenario

Figure 10 shows the end-to-end delay of the direct communication scenario under optimal conditions. These optimal conditions are clearly visible in the graph, since approximately 83% of the critical bundles arrive at the first mark and within a maximum of 3 s even every critical bundle has arrived. Not far below are the curves of the normal and the FIFO bundles. Their course is rather similar with even occasional overlaps. The FIFO bundles arrive with a chance of 70% within 2.5 s and are only slightly lower than the normal bundles with 73%. At the reach of 100% they overlap at around 4.6 s. The curve of the bulk bundles is below the FIFO and the normal curves. It reaches the limit of 2.5 s with a probability of 62%, and the limit of 5 s with exactly 100%, ensuring that all bulk bundles also arrive within the limits. Overall, although the number of losses is low, traffic prioritization still has a positive impact on the critical bundles. This comes at the expense of the bulk, but especially in such optimal conditions, this does not demand a great trade-off, since all bundles arrive within the limits regardless of their priority.

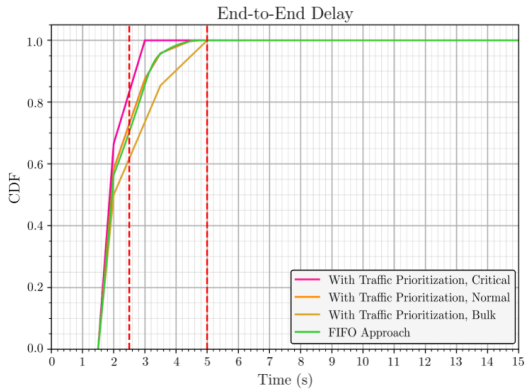

Figure 10. End-to-End Delay in the One-Hop Scenario with Optimal Conditions

With average conditions the probability of critical bundles arriving within 2.5 s decreased compared to optimal conditions and is now 73%. The decrease of normal (60%) and FIFO (48%) bundles is slightly greater. The bulk probability shows a bigger decline achieving a probability of 43% with average conditions. It is also the only curve not reaching 100% before 12 s showing the high impact of the worsened conditions on the bulk bundles, since the interference from high priority bundles increased the

waiting time of the low priority classes. As the losses remain manageable, as evidenced by 98% of critical bundles arriving before the second mark, the impact on the normal bundles is less significant. 92% of the normal bundles still arrive within the limits, which is rather high, especially comparing both the critical and the normal percentages with the FIFO approach, where only 85% arrive before the second mark. Even with this interference from high priority bundles, 74% of bulk arrive before 5 s, which is still a good outcome. The resulting trade-off yields a performance gain, with both the critical and normal showing higher efficiency compared to the FIFO baseline.

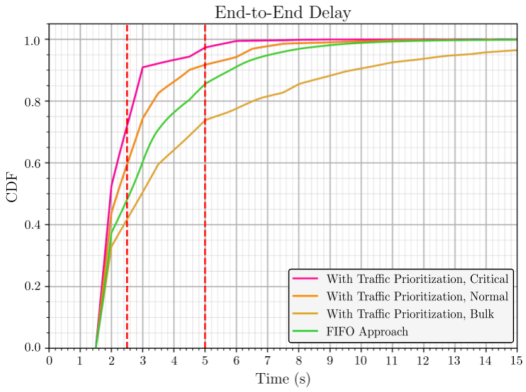

Figure 11. End-to-End Delay in the One-Hop Scenario with Average Conditions

The end-to-end delay displayed in Figure 11 shows high similarities with the results of the experiment with 3 priority classes of Algarra et al. [6]. Therefore, the split of the environments did not change the overall modeling of the direct communication link too much to receive similar results as with the single environment. Furthermore, the results from the two- or three-hop scenarios are applicable to the research of Algarra, providing validation for their findings.

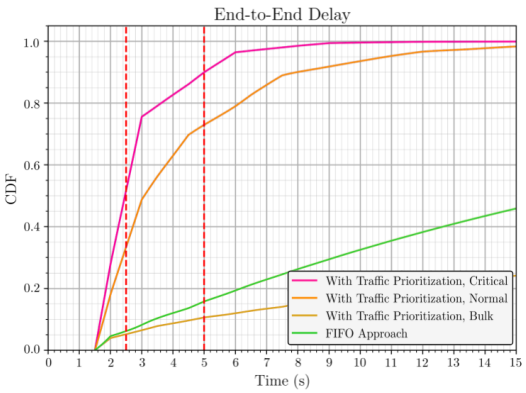

Figure 12. End-to-End Delay in the One-Hop Scenario with Worst Conditions

The higher percentages of loss present in the worst conditions can be seen in the end-to-end delay displayed in Figure 12. Only 52% of the critical bundles arrive at the 2.5 s mark, but 90% arrive before the 5 s mark. While the conditions do dampen the performance of the critical bundles, the resulting arrival rate still represents a satisfactory outcome. The performance of the normal bundles is less favorable compared to the critical bundles, with 53% delivered before the first mark and 73% before the second mark. FIFO and bulk bundles demonstrate an even poorer performance, with their curves showing an almost linear progression and only a very slight increase over time. Only 5% of the bulk bundles arrive before the 2.5 s mark and for FIFO it is only a slightly higher percentage. Even at the second mark, the values did not significantly increase. FIFO achieves 16%, while bulk only gets to 6%. After 15 s both curves did not reach 50% of transmitted bundles.

B. Two-Hop Scenario

The overall delay of the two-hop scenario with optimal conditions can be seen in Figure 13. A high similarity with the end-to-end delay from the optimal one-hop scenario is visible, because the critical bundles dominate the graph, while normal and FIFO overlap and bulk is located below them. Therefore, the results remain good, but critical now reaches the first mark at 76%, normal at 65%, FIFO at 62%, and bulk at 55%, which means a drop of around 8% for all classes. Associated with the similarity to the one-hop scenario are also the conclusions drawn from it, meaning that traffic prioritization keeps its positive impact even under optimal conditions and even in a multi-hop scenario. Additionally, the trade-off did not worsen the overall results, since all bundles still arrive with 100% probability within the limits.

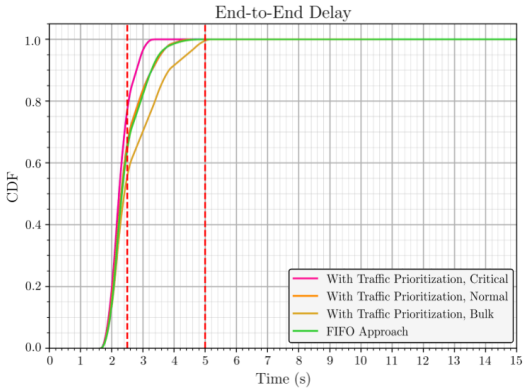

Figure 13. End-to-End Delay in the Two-Hop Scenario with Optimal Conditions

The performance characteristics of the two-hop scenario with average conditions in Figure 14 show that the normal and FIFO curves are much closer now compared to the one-hop scenario. However, the probabilities at the first mark decreased for all curves due to the higher losses. Critical decreased from 76% to 65%, normal from 65% to 55%, FIFO from 62% to 53% and bulk from 55% to 45%. Additionally, the curves do not reach 100% within the limits anymore, but all continue to get above 85%. Even

though the conditions got worse and an additional hop was included, the critical bundles keep outperforming the FIFO approach on the expense of the bulk bundles. The curve of the critical bundles is very steep, showing that even if the total propagation delay is now longer because of the two hops, traffic prioritization remains a positive impact. The higher loss because of multiple hops is a hindrance especially for critical bundles that should be researched further.

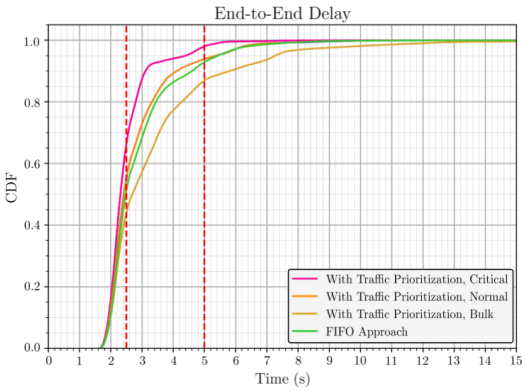

Figure 14. End-to-End Delay in the Two-Hop Scenario with Average Conditions

In Figure 15 the end-to-end delay of the two-hop scenario with worst conditions can be seen. Again similarities to the one-hop worst-case scenario are visible, but with an overall drop in percentages. Critical is now at 50% at the first mark, normal at 38%, FIFO at 30% and bulk at 25%. The pattern already observed from the previous scenarios continue here, supporting the preference of the highest priority class. However, the transmission over two hops appears to have improved the relative performance of the FIFO approach and bulk, since they were far below the other curves in the one-hop scenario.

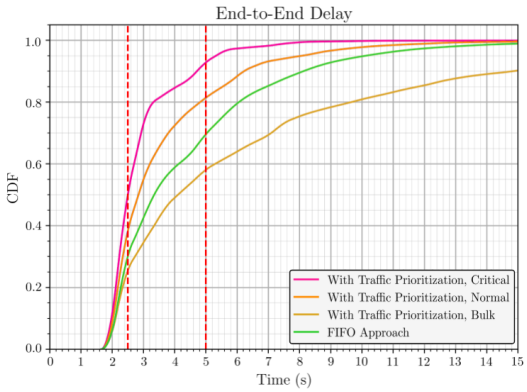

Figure 15. End-to-End Delay in the Two-Hop Scenario with Worst Conditions

Across all conditions, the validation of the better performance of critical bundles at the expense of low priority bundles continues to be demonstrated in the results.

C. Three-Hop Scenario

Looking at Figure 16 the three-hop scenario with optimal conditions shows similarities to the two-hop scenario. The curves have an alike shape, with the greatest parallels being with the FIFO and normal curves. However, the percentages of these curves are still different, since their origin is not at 1.6 s, but at around 2 s, because the higher servicing time shifts the origin in the final graph. Since the curves are all rather close to each other when hitting the first mark, a direct assignment of each class to its probability is hardly possible. The area of impact is from 23% to 33%, which is a significant decrease from the previous 76%, 65%, 62% and 55%. However, before the second mark all curves reached 100% except for the bulk being at 96%. Even though the first percentages are rather low, the positive impact of traffic prioritization continues to be shown, since it outperforms all other classes. Although, the high impact of the service time makes the target mark hard to reach even in optimal conditions.

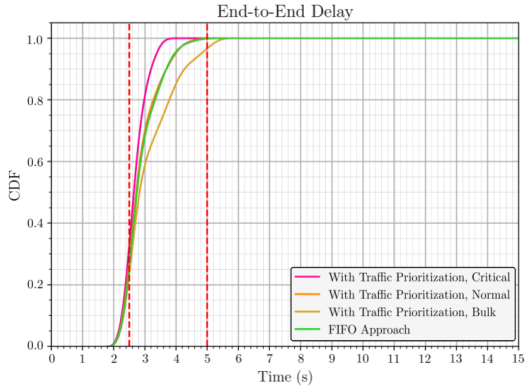

Figure 16. End-to-End Delay in the Three-Hop Scenario with Optimal Conditions

Before analyzing the overall end-to-end delay in the three-hop scenario with average conditions, the delay of each hop is shown first in Figure 17. These separated delays are especially interesting in the three-hop scenario, because each hop only corresponds to one environment, which allows for deductions about the atmospheric and space setting. The similarities of these three graphs to the ones of optimal and worst case are very high, with only small degradations, which is why only for average conditions this split is shown.

For the first hop the origin of all curves is now 0.4 s, since the bundle service time depends on the distance. From there it is a very steep curve to 100%, which is reached by the critical bundles at 2.2 s, for normal at 2.3 s and for bulk at 2.7 s. In the second hop critical arrives at the first mark at 99%, normal at 88% and bulk at 75%. These two plots show the impact of the losses in space on the delay. It becomes clear from the second hop that the impact increases proportionally with the distance. The plot of the third hop then shows the low impact of the atmospheric losses, since all curves are overlapping.

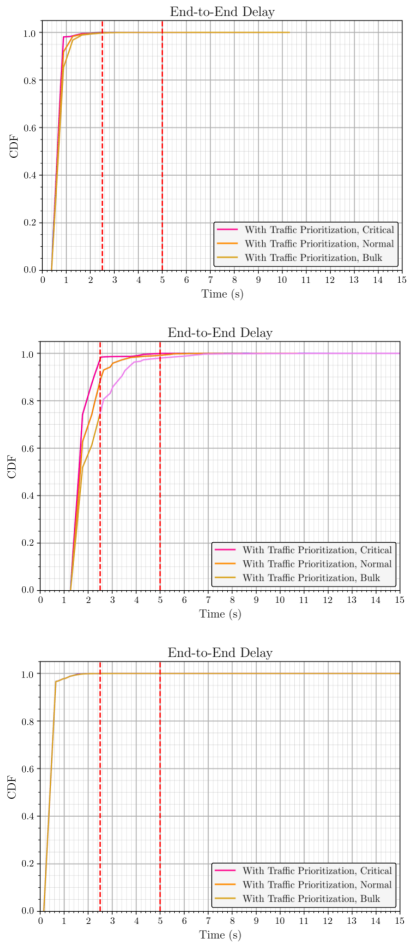

Figure 17. Breakdown of the End-to-End Delay per Hop in the Three-Hop Scenario with Average Conditions

Resulting from these plots, the end-to-end delay displayed in Figure 18 only shows small changes compared to the optimal case. The area of impact with the 2.5 s mark did not change noticeably. However, the small changes in all three-hop delays are obvious in this graph, since no curve reaches 100% before the second mark now. Additionally, all curves are slightly lower in rise such that the probabilities at the 5 s mark are 99% for critical, 98% for FIFO and normal, and 83% for bulk. Therefore, the higher error rates are displayed in the delays even though the overall graph is not very different from the optimal case. This suggests that the influence of the error rates on the delay of each bundle decreases with increasing number of hops. A fitting explanation would be the lower service times, which allow for faster reaction to losses. This shortens the time until retransmission, resulting in a higher throughput, which also benefits the lower priorities. Furthermore, the distribution of the priority classes over all nodes becomes more balanced such that all bundles have a good chance of being sent regardless of their priority class. Based on this analysis, the changes under the worst conditions should be minimal again, following the trend set in the two-hop scenario, which showed minimal differences between the optimal and the average conditions.

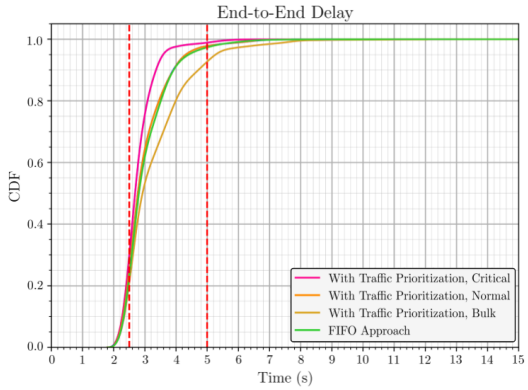

Figure 18. End-to-End Delay in the Three-Hop Scenario with Average Conditions

The end-to-end delay of the worst conditions also only shows small changes to the average conditions, as can be seen in Figure 19. However, the normal and the FIFO approach develop some separation, reestablishing the general order of curves. Because of the higher losses, the area of impact with the first mark is set slightly lower than before at 18% to 33%. The curves reach the second mark at 97% for critical, 94% for normal, 93% for FIFO and 86% for bulk.

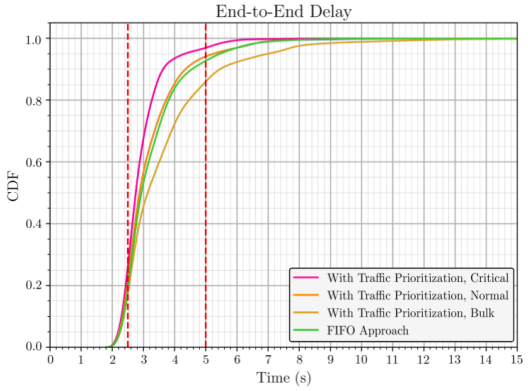

Figure 19. Comparison of the End-to-End Delay in the Three-Hop Scenario with Worst Conditions

These results support the hypothesis that a higher number of hops weakens the influence of losses on the end-to-end delay, because of the higher throughput of each node. Additionally, if a sending attempt of a low priority bundle is already started, it does not get interrupted even if a higher priority bundle arrives, which could contribute to a better throughput for low priority bundles. Nevertheless, the positive impact of traffic prioritization remains visible even with these findings. The critical class arrives even under worst conditions and over multiple hops faster at the destination than the FIFO bundles.

D. Evaluation

The findings from all experiments have been systematically analyzed to provide comprehensive insights into traffic prioritization performance across multi-hop scenarios. Therefore, a comprehensive summary of all insights will confirm or refute the drawn conclusions, and allows for statements that span all experiments.

The main goal of the experiments was to analyze the impact of traffic prioritization not only on a one-hop, but also on a multi-hop path. First, the validation of the results of the work of Algarra et al. [6] had to be performed. In the analysis of the one-hop scenario with average conditions, strong similarities appeared to their work. Therefore, the changes to the Markov chain in this thesis were not so drastic that the results of Algarra's work are not comparable anymore. Thus, their approach, although less detailed in its losses compared to this work, still adequately represented the Earth-to-Moon communication link. These similarities result in an applicability of the findings from the multi-hop scenarios to the work of Algarra.

The overall outcome of the traffic prioritization evaluation is a clear performance improvement for the critical bundles. In all experiments regardless of the conditions or number of hops, the critical class always performed better than all other classes, and especially compared to the FIFO approach. The extent of the improvement depends on the condition and number of hops. It is for example significantly higher for a one-hop case with worse conditions than with optimal conditions, resulting from the overall loss experienced being generally higher, such that the urgency of the critical class proves more useful.

In the comparison of the performance improvements of the critical bundles, it was discovered that the higher the number of hops, the lower the improvement. This is presumably because of lower service time at each hop, resulting in a faster retransmission attempt. Stemming from that is also a higher spread of bulk bundles over multiple hops, such that the lower priorities are serviced due to lack of higher priority bundles. Overall, the delay increased for all classes as more hops were involved, since each hop introduced an additional service time and an additional transmission attempt to pass. This service time decreased the percentage of bundles arriving before the 2.5 s mark especially for the high priority bundles.

Combining those two insights, it becomes apparent that a change in the routing according to the priority class of the bundle might provide improvement. Critical bundles should be sent as directly as possible to their destination to avoid multiple service times and minimize the risk of being blocked by potential loss more than once. However, low priority bundles may be routed through multiple hops to have them distributed widely in the network improving their chances of being serviced next and of not being blocked by a higher priority bundle. If the communication is only possible over multiple hops, it might be beneficial to interrupt the transmission of a low priority bundle in favor of a critical bundle to enhance the transmission time of the high priority bundles.

Apart from findings about traffic prioritization, it also became apparent that the space setting has a much higher influence on the communication link than the atmospheric setting. This is particularly noticeable in the three-hop scenarios, where each hop was assigned to exactly one setting, and therefore the delay plot of the atmospheric setting showed a very low impact. The second hop, in the three-hop scenario, however, displayed the highest delay, since the distance of that hop was the largest, resulting in a bottleneck. In this case interrupting low priority transmissions upon the arrival of high priority bundles might be desirable as well to decrease the delay for critical bundles.

VI. Conclusion and Future Work

A. Conclusion

The communication infrastructure between Earth and Moon needs to develop in order to be able to support all the planned upcoming missions [8]. However, to support this development more robust and reliable communication mechanisms need to be in place. As of now the DTN with BP is envisioned to be the future standard for space communications because of its hop-by-hop approach fitting for the highly stressed communication environment that this setting presents. However, it lacks QoS mechanisms to maximize the utilization of limited bandwidth, provide reliability and be able to achieve the delivery time requirements.

Traffic prioritization is a QoS mechanism fitting for handling limited resources, and so the overall goal of these experiments was to evaluate the impact of traffic prioritization on multi-hop paths building on previous work [6]. All experiments regardless of the scenario or the conditions demonstrated a performance improvement of critical bundles compared to FIFO. The implementation of traffic prioritization into the BP is therefore recommended based on this study. The highest gain is achieved in a one-hop scenario with worst conditions. Throughout the two- and three-hop scenario the gain is reduced whereas the performance of the low priority bundles increased. This is due to the lower service time enabling faster retransmission attempts, which, in turn, lead to a better distribution of bulk bundles, increasing their probability of being serviced. Based on these findings, the suggestion is to additionally adjust the routing of the bundle according to its priority class, which would benefit not only the high priority bundles, but also the low priority ones. The critical bundles should therefore be sent via the most direct route possible to the destination, whereas the bulk bundles can alternatively traverse through multiple nodes on their way. However, it is not uncommon that one node in the path is a critical congestion point, such that all bundles travel through it, creating a bottleneck. The research showed in

the three-hop scenario the significant influence bottlenecks can have on all classes. In such cases the dropping of a low priority class bundle might be desirable in favor of a high priority bundle, such that the effect of the bottleneck is mitigated for the critical bundles.

B. Future Work

The effect of routing according to the bundle's priority as well as the preemptive dropping of a low priority bundle in favor of a high priority bundle requires individual research studies to validate its potential. In addition, the work on prioritization is not yet complete, missing a deployment to a satellite or spacecraft and an analysis of the resulting findings to identify as the actual gains or potential issues. In preparation for deployment, more experiments with the constructed Markov chain could be conducted, testing a different traffic distribution more representative of realism. Additionally, the approach of using weighted queuing instead of strict prioritization as researched in Algarra et al. [6] would provide valuable insights and might further validate the existing results for a multi-hop path.

Moreover, further research on the model would also be beneficial. All data used for the probabilities of the Markov chain were carefully researched. However, in some areas a lack of information made fine-tuning challenging, as for example the entry probability for clouds, which is based on the number of rainy days rather than cloudy days. A purpose-oriented gathering of data would make these values more realistic. Additionally, some loss factors were not included as to reduce the complexity of the model, but might be a valid addition depending on its application area for scenarios in which a highly realistic model is needed.

The Markov model can also be used for the research of additional QoS mechanisms. Especially for reliability, only the implementation was investigated but a study on its actual benefits for the communication link was not provided. The usage of the communication link will increase in the future, such that its improvement is essential.

Beyond testing new features for the link, the Markov chain could also be used for a general study of the Moon-to-Earth communication link. An additional step for that could be the modification to support flexible transmission links instead of a hard coded FSO link through the atmospheric setting and RF link through space. With that, the current state of the link in combination with different scenarios and conditions might provide insights into routing or the types of loss influencing the transmission the most, such that further work can be done on prevention. An alternative to prevention is the correction of errors. By treating the bundles as bits, such error correction algorithms could be tested for their performance in the Moon-to-Earth communication link and optimized with the information gained. The model's realistic depiction can also provide information about actual transmission times. The program could be modified to add contact windows, so that no continuous communication is assumed. Combining the contact windows with the losses would yield the actual success communication availability timeframes.

Overall, the research into lunar communications and therefore the importance of the Moon-to-Earth communication link will continue to grow in the coming years. Therefore, improvements such as traffic prioritization are crucial to ensure the success of the missions. The demonstration of the performance gain should result in an implementation of traffic prioritization into BP, permanently enhancing the communication link. Additionally, the flexible model of a multi-hop transmission path will remain relevant and prove useful in future research.

References

[1] K. Schaper, T. A. Ulierte, A. Timm-Giel, and F. Flentge, "Modeling of multi-hop dtn-based lunar communications for the evaluation of traffic prioritization", in *Proceedings of the Seventeenth International Conference on Advances in Satellite and Space Communications*, Available: https://personales.upv.es/thinkmind/SPACOMM/SPACOMM_2025/spacomm_2025_1_20_20015.html [accessed Nov. 15, 2025], IARIA, May 2025, pp. 5–11.

[2] J. M. Logsdon, *Space exploration*, Available: https://www.britannica.com/science/space-exploration [accessed Dec. 08, 2024], Encyclopedia Britannica, Nov. 2024.

[3] F. Warthman, "Delay- and disruption-tolerant networks (dtns), A tutorial", Tech. Rep., Sep. 2015, Available: https://www.nasa.gov/wp-content/uploads/2023/09/dtn-tutorial-v3.2-0.pdf [accessed Nov. 15, 2025].

[4] European Space Agency, *Gateway: Lunar link*, Available: https://www.esa.int/Science_Exploration/Human_and_Robotic_Exploration/Gateway_Lunar_Link [accessed Dec. 08, 2024].

[5] CDF Lunar Caves Study team, *Lunar caves cdf study - executive summary*, Available: https://esamultimedia.esa.int/docs/preparing_for_the_future/Lunar_Caves_Executive_Summary_1.0.pdf [accessed Nov. 15, 2025], European Space Agency, Mar. 2022.

[6] T. Algarra Ulierte, K. Kuladinithi, A. Timm-Giel, and F. Flentge, "Adding quality of service support to bundle protocol through an extension block", in *2024 IEEE 10th International Conference on Space Mission Challenges for Information Technology (SMC-IT)*, 2024, pp. 115–124. DOI: 10.1109/SMC-IT61443.2024.00020.

[7] T. Algarra Ulierte, K. Kuladinithi, A. Timm-Giel, and F. Flentge, "Lunar communication services: Feasibility study on traffic prioritization of quasi-real time communications over dtns", in *2023 IEEE International Conference on Wireless for Space and Extreme Environments (WiSEE)*, IEEE, Sep. 2023, pp. 35–40. DOI: 10.1109/wisee58383.2023.10289636.

[8] Lunar Communications Architecture Working Group, "The future lunar communications architecture", Interagency Operations AdvisoryGroup, Tech. Rep., Jan. 2022.

[9] E. Birrane III and K. McKeever, *Rfc 9172: Bundle protocol security (bpsec)*, 2022.

[10] T. Algarra Ulierte, F. Flentge, J. Quintanilla, and A. Timm-Giel, "Characterizing space communication channel behavior: An analytical approach with esa mission data validation", in *10th ESA International Workshop on Tracking, Telemetry and Command Systems for Space Applications (TT&C)*, 2025.

[11] K. Scott and S. C. Burleigh, *Bundle Protocol Specification*. Nov. 2007. DOI: 10.17487/rfc5050.

[12] Consultative Committee for Space Data Systems, *Bundle protocol specification (ccsds 734.2-b-1)*, Sep. 2015.

[13] S. Burleigh, "Interplanetary overlay network: An implementation of the dtn bundle protocol", in *2007 4th IEEE Consumer Communications and Networking Conference*, IEEE, Jan. 2007, pp. 222–226. DOI: 10.1109/ccnc.2007.51.

[14] P. Apollonio, C. Caini, and V. Fiore, "From the far side of the moon: Delay/disruption-tolerant networking communications via lunar satellites", *China Communications*, vol. 10, no. 10, pp. 12–25, Oct. 2013, ISSN: 1673-5447. DOI: 10.1109/cc.2013.6650316.

[15] H.-P. Lin, M.-J. Tseng, and D.-B. Lin, "Modeling fading properties for mobile satellite link channels using markov model approaches", vol. 4, 192–195 vol.4, 2003. DOI: 10.1109/APS.2003.1220153.

[16] J. Bitó, "On the markov modeling of digital communication channels", in *2008 IEEE 19th International Symposium on Personal, Indoor and Mobile Radio Communications*, IEEE, 2008, pp. 1–6.

[17] M. Tropea and F. De Rango, "A comprehensive review of channel modeling for land mobile satellite communications", *Electronics*, vol. 11, no. 5, p. 820, 2022.

[18] F. P. Fontan *et al.*, "Complex envelope three-state markov model based simulator for the narrow-band lms channel", *International journal of satellite communications*, vol. 15, no. 1, pp. 1–15, 1997.

[19] V. Chu, P. Sweeney, J. Paffett, and M. N. Sweeting, "Characterising error sequences of the low earth orbit satellite channel and optimisation with hybrid-arq schemes", in *IEEE GLOBECOM 1998 (Cat. NO. 98CH36250)*, ser. GLOCOM-98, vol. 5, Sydney, NSW, Australia: IEEE, 1998, pp. 2930–2935. DOI: 10.1109/glocom.1998.776610.

[20] X. Pan, Y. Zhan, P. Wan, and J. Lu, "Review of channel models for deep space communications", *Science China Information Sciences*, vol. 61, no. 4, p. 040 304, Mar. 7, 2018, ISSN: 1869-1919. DOI: 10.1007/s11432-017-9345-8.

[21] T. Algarra Ulierte, F. Flentge, and A. Timm-Giel, "Quality of service extension for delay- and disruption-tolerant networking", in *18th International Conference on Space Operations (SpaceOps)*, 2025.

[22] T. Algarra Ulierte, K. Kuladinithi, A. Timm-Giel, and F. Flentge, "Enabling traffic prioritization for space communications over dtns", *IEEE Journal of Radio Frequency Identification*, vol. 8, pp. 748–760, 2024, ISSN: 2469-729X. DOI: 10.1109/jrfid.2024.3415508.

[23] C. Barry, *Weather on the moon*, Blog, Available: https://science.nasa.gov/moon/weather-on-the-moon/ [accessed Nov. 15, 2025], National Aeronautics and Space Administration.

[24] B. Yost and S. Weston, "State-of-the-art of small spacecraft technology", in National Aeronautics and Space Administration, Feb. 2024, ch. 9 Communications, pp. 243–271, Available: https://ntrs.nasa.gov/citations/20240001462 [accessed Nov. 15, 2025].

[25] European Space Agency, *What are solar flares?*, Blog, Available: https://www.esa.int/Science_Exploration/Space_Science/What_are_solar_flares [accessed Nov. 21, 2024].

[26] European Space Agency, *Optimised ccsds protocol stack for high data rate (erasurevectors)*, Login required.

[27] M. Hatfield, *Solar flares faqs*, Available: https://blogs.nasa.gov/solarcycle25/2022/06/10/solar-flares-faqs/ [accessed Dec. 14, 2024], National Aeronautics and Space Administration, Jun. 2022.

[28] N. Nishizuka, Y. Kubo, K. Sugiura, M. Den, and M. Ishii, "Reliable probability forecast of solar flares: Deep flare net-reliable (defn-r)", *The Astrophysical Journal*, vol. 899, no. 2, p. 150, Aug. 2020, ISSN: 1538-4357. DOI: 10.3847/1538-4357/aba2f2.

[29] Y. Guo *et al.*, "Feature identification and statistical characteristics of quasi-periodic pulsation in solar flares using the markov-chain-monte-carlo approach", *The Astrophysical Journal*, vol. 944, no. 1, p. 16, Feb. 2023, ISSN: 1538-4357. DOI: 10.3847/1538-4357/acb34f.

[30] Consultative Committee for Space Data Systems, "Real-time weather and atmospheric characterization data (ccsds 140.1-g-2)", Tech. Rep. Issue 2, Mar. 2024, Available: https://public.ccsds.org/Pubs/140x1g2.pdf [accessed Nov. 15, 2025].

[31] World Weather & Climate Information, *Monthly average rainy days in santa maria*, Available: https://weather-and-climate.com/average-monthly-Rainy-days,santa-maria-cv,Cape-Verde [accessed Dec. 14, 2024].

[32] Climates To Travel, *Climate in kiruna (sweden)*, Available: https://www.climatestotravel.com/climate/sweden/kiruna [accessed Dec. 14, 2024].

[33] World Weather Online, *Kourou annual weather averages*, Available: https://www.worldweatheronline.com/kourou-weather-averages/gf.aspx [accessed Dec. 14, 2024].

[34] I. A. Lund, "Persistence and recurrence probabilities of cloud-free and cloudy lines-of-sight through the atmosphere", *Journal of Applied Meteorology*, vol. 12, no. 7, pp. 1222–1228, Oct. 1973, ISSN: 0021-8952. DOI: 10.1175/1520-0450(1973)012<1222:parpoc>2.0.co;2.

[35] Team SimPy, *Overview - simpy documentation*, Available: https://simpy.readthedocs.io/en/latest/ [accessed Nov. 29, 2024].